Trusted Position for 5G-Connected Urban Robots Based on LiDAR-IMU Detection and QPV-Based Verification Bounds

İsmail Eren Küçükali*[1,3], Paweł Buksakowski[2,4], Laia Pages[1], Marc Jofre[3], and Luis Jofre[4]

[1]CARNET Barcelona – The Future Mobility Research Hub, Nexus II Building – Office 0A, C/ Jordi Girona, 29, 08034 Barcelona, Spain
[2]Institute of Radiocommunications, Faculty of Computing and Telecommunications, Poznań University of Technology, 60-995 Poznań, Poland
[3]Department of Network Engineering, Universitat Politècnica de Catalunya – BarcelonaTech (UPC), 08860 Castelldefels (Barcelona), Spain
[4]CommSensLab, Department of Signal Theory and Communications (TSC), Universitat Politècnica de Catalunya – BarcelonaTech (UPC), Campus Nord, 08034 Barcelona, Spain

Short Summary

Urban service robots in dense urban centers require reliable onboard perception and a trustworthy position claim within connected mobile infrastructure. This work presents a Trusted Position framework integrating a validated lightweight dynamic obstacle detection (DOD) pipeline with 5G connectedness characterization using ns-3/5G-LENA multi-cell simulations under realistic SUMO-based mobility. Quantum Position Verification (QPV) is incorporated as an abstract timing-constrained positional authentication layer. The DOD pipeline sustains 10-15 Hz operation with high static filtering accuracy. Network simulations reveal a throughput-timeliness trade-off: TDMA (Time-Division Multiple Access) schedulers maintain sub-10 ms delivery, whereas OFDMA (Orthogonal Frequency-Division Multiple Access) schedulers increase delays to 85-1505 ms, exceeding freshness budgets for local perception coherence. The results define three trust levels: TDMA trusted, OFDMA MR (Maximum Rate) conditionally trusted, and OFDMA PF (Proportional Fair)/RR (Round Robin) untrusted. Under the studied conditions, the proposed trusted positioning is achievable with TDMA within the proposed timing-bound model.

Keywords: 5G; LiDAR-IMU; Urban Mobility; Obstacle Detection; Network Latency; Quantum Position Verification

1 Introduction

Autonomous urban service robots operating on sidewalks and plazas must perceive dynamic obstacles reliably while maintaining a trustworthy position claim within connected mobility infrastructure Rosique et al. (2019); Leong & Ahmad (2024). This work focuses on ONA, an autonomous urban service robot deployed in Barcelona for last-mile logistics in complex public spaces. Figure 1 illustrates ONA in a representative city-center environment.
A lightweight LiDAR-IMU (Inertial Measurement Unit) DOD and tracking pipeline, validated on ONA in real urban deployments Küçükali et al. (2025), provides on-board real-time situational context without external maps or cloud offloading Sualeh & Kim (2020); Du & Beltrame (2024). Although on-board DOD operates independently of communication, Trusted Position in connected robotics is constrained by network timeliness. In 5G New Radio (NR), end-to-end latency and jitter vary with load, user density, and scheduling policy 5G-LENA Project (2019); a position claim that is correct on-board may become stale once communication delay exceeds the robot's local update rhythm. Therefore, this work examines how 5G connectedness bounds the timeliness of position-related interactions and shapes a system-level notion of Trusted Position under realistic urban vehicular mobility modelled via SUMO (Simulation of Urban Mobility) Lopez et al. (2018). QPV adds timing-sensitive verification constraints grounded in the laws of quantum information and relativistic signaling: when delay variability exceeds the admissible verification



Figure 1: The ONA autonomous urban robot operating in Barcelona city.

window, verification feasibility degrades, and the same delay statistics determine whether positional verification remains feasible Miller & Alnawakhtha (2024); Kent et al. (2011). No prior work jointly addresses LiDAR-based urban robot perception Rosique et al. (2019); Leong & Ahmad (2024); Sualeh & Kim (2020); Du & Beltrame (2024), 5G NR scheduling 5G-LENA Project (2019); Trabelsi et al. (2024), the Age of Information framework Kaul et al. (2012), and QPV protocols Kent et al. (2011); Miller & Alnawakhtha (2024), or frames temporal coherence as a position-trust constraint with a QPV-inspired verification bound. Four contributions follow. First, a cross-layer Trusted Position framework connects perception refresh rhythm, 5G delay statistics, and QPV-based verification feasibility through freshness. Second, a validated DOD baseline establishes the 10-15 Hz refresh rate as the reference for freshness and QPV analysis. Third, a 5G connectedness envelope quantifies how access mode (TDMA vs. OFDMA) and scheduler policy (RR, PF, MR) shape delay and fairness under urban vehicular mobility. Fourth, freshness and QPV feasibility analysis yields a three-tier trust classification: trusted, conditionally trusted, and untrusted, with practical design guidelines for 5G-connected urban robot deployments.

2 Methodology

This work follows a three-layer structure. The first layer is a validated LiDAR-IMU DOD pipeline running fully on ONA, providing the refreshed local situational context used by subsequent layers. The second layer characterizes the 5G connectedness envelope using ns-3/5G-LENA simulations on a five-gNB (next-generation NodeB) cross topology at 3.5 GHz with 20 MHz bandwidth, μ=2 numerology, and downlink-dominated TDD (Time-Division Duplex), with user mobility driven by SUMO-generated urban vehicle traces under high-density conditions. The third layer introduces an abstract QPV timing constraint as a verification-bound signal governed by the same delay statistics.

LiDAR-IMU Dynamic Obstacle Detection Baseline on ONA

The perception baseline is a lightweight, real-time DOD and tracking pipeline implemented in ROS (Robot Operating System) and executed fully on-board the ONA robot. Two 64-channel 3D LiDARs provide 360° coverage, complemented by IMU measurements for ego-motion compensation. Table 1 summarizes the sensing configuration and Figure 2 outlines the five processing stages from point cloud fusion through to dynamic tracking.
The pipeline operates in five stages. Stages 1-3 perform LiDAR fusion, RANSAC-based

Table 1: ONA perception sensor configuration (DOD baseline).

Sensor	**Role in pipeline**
2× 3D LiDAR (64-ch)	360° point cloud acquisition and fusion
2× IMU	Ego-motion / yaw-rate compensation and alignment

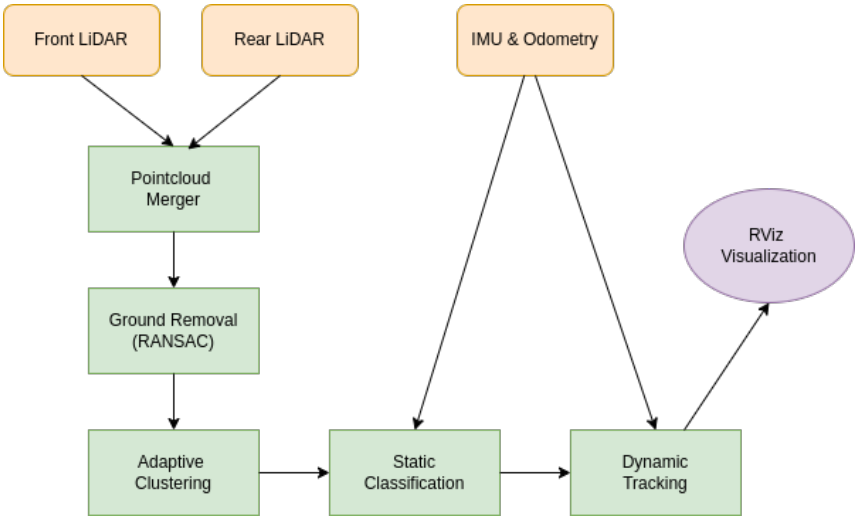


Figure 2: System overview of the on-board LiDAR-IMU DOD pipeline on ONA (adopted from Küçükali et al. (2025)).

ground removal, and range-adaptive Euclidean clustering with band-dependent tolerance ϵ_k Li et al. (2021); Cibir et al. (2024); Jiang et al. (2023); Lin et al. (2024). Stage 4 applies ego-motion-aware static filtering using odometry translation Δx_t, Δy_t and yaw θ_t:

$$\tilde{c}_{t-1} \;=\; \mathbf{R}(\theta_t)\Big(\mathbf{R}(-\theta_{t-1})\, c_{t-1} - [\Delta x_t,\, \Delta y_t]^\top\Big)\,, \tag{1}$$

where $\mathbf{R}(\cdot)$ is a 2D rotation matrix. Omitting this stage drops tracking accuracy from ∼50% to ∼20% Küçükali et al. (2025); Xie et al. (2019). Stage 5 tracks non-static clusters with a Kalman filter under a constant-velocity state

$$\mathbf{x}_t = \begin{bmatrix} x_t & y_t & z_t & \dot{x}_t & \dot{y}_t & \dot{z}_t \end{bmatrix}^\top, \tag{2}$$

and Hungarian-algorithm data association Mills-Tettey et al. (2007), with yaw-rate compensation applied to absolute velocity estimates Küçükali et al. (2025), where (x_t, y_t, z_t) denote the 3D position of the tracked object in the robot reference frame and $(\dot{x}_t, \dot{y}_t, \dot{z}_t)$ its linear velocity components under a constant-velocity motion assumption.
The validated pipeline establishes $T_{\mathrm{DOD}} \approx 0.067$–$0.10$ s as the timing reference for Section 3. Hence, position trust degradation is primarily driven by network-side delay and temporal jitter.

5G Connectedness Characterization with ns-3/5G-LENA

The communication timeliness shell (delay, jitter, loss, and fairness) is characterized using the ns-3/5G-LENA NR simulator to bound the freshness of position-related interactions: periodic position claims, supervisory queries, and safety notifications 5G-LENA Project (2019).

Network Topology and Radio Configuration

Five gNBs are arranged in a cross topology (Figure 3): one central macro gNB at $(0, 0)$ with 25 m antenna height and four pico cells at (±250 m, 0) and (0, ±250 m) with 10 m

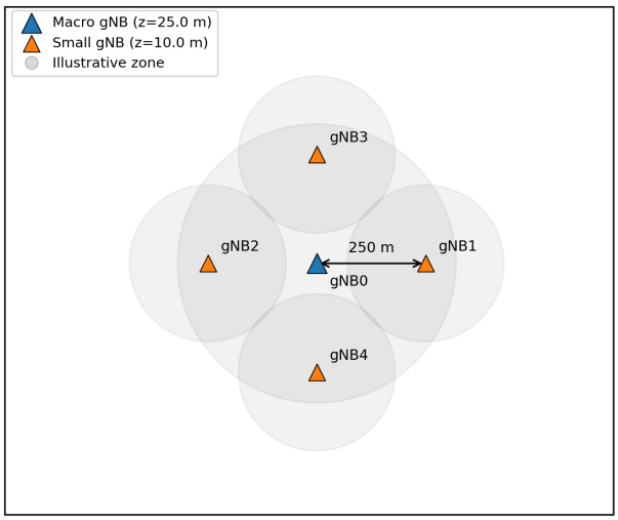


Figure 3: Multi-cell 5G NR simulation scenario: five-gNB cross topology (one macro gNB at center, four pico gNBs at ±250 m) with EPC (Evolved Packet Core)/remote-host connectivity. UE (User Equipment) mobility follows SUMO-generated vehicle traces integrated via a frame-by-frame mobility driver.

height, all connected to an EPC which interfaces with a remote host via the SGi interface. All cells operate at 3.5 GHz with 20 MHz bandwidth, μ=2 numerology, and a downlink-dominated TDD pattern. UE attachment follows best-signal cell selection; handovers use an A3 RSRP (Reference Signal Received Power)-based algorithm with X2 signalling 3GPP (2021).

Mobility Model

User mobility is represented through SUMO-generated vehicle trajectories constrained by an urban road network, with 150 concurrent UEs to reflect high-density urban conditions consistent with the Barcelona city-center context Lopez et al. (2018). This load ensures that the characterization captures significant resource contention and inter-cell interference, providing a stress-test baseline for the Trusted Position framework. A dedicated mobility driver updates UE positions frame-by-frame within ns-3, ensuring cell association, interference, and radio quality evolve dynamically across each run.

Traffic and QoS Configuration

Downlink traffic is modelled as UDP (User Datagram Protocol) CBR (Constant Bit Rate) streams from a RemoteHost via the SGi interface, with dedicated EPS (Evolved Packet System) bearers mapping application flows to RLC (Radio Link Control)-level QoS (Quality of Service) entities. Traffic generation per UE is delayed until a valid RRC (Radio Resource Control) connection and RNTI (Radio Network Temporary Identifier) assignment are confirmed, followed by a one-second guard interval. FlowMonitor collects per-flow statistics: mean delay μ_D, jitter J, packet loss, and throughput. MAC-layer (Medium Access Control) traces enable computation of cell-level throughput and the dual-level Jain fairness index Jain et al. (1984).

Schedulers Under Evaluation

RR, PF, and MR policies are evaluated under both TDMA and OFDMA access modes, yielding six scheduler configurations. In TDMA mode, all RBGs (Resource Block Group) within a symbol interval are allocated to a single UE; in OFDMA mode, RBGs are distributed across multiple UEs within the same interval, enabling finer frequency-domain

Table 2: Baseline simulation parameters (High-density urban scenario).

Parameter	**Value**
Topology	5-gNB cross (1 macro + 4 pico)
User Density	150 UEs (SUMO-based)
Mobility	SUMO urban vehicle traces
Carrier / Bandwidth	3.5 GHz / 20 MHz
Numerology / TDD	μ=2 / DL-heavy TDD
Schedulers	TDMA & OFDMA × {RR, PF, MR}
Traffic	UDP CBR, dedicated EPS bearers
Simulation duration	180 s
KPI (Key Performance Indicator) collection	FlowMonitor + MAC DlScheduling traces

granularity Trabelsi et al. (2024). All runs use identical topology, mobility, and traffic parameters; only the scheduler varies between runs. Table 2 summarizes the baseline simulation parameters.

Freshness-Bounded Trusted Position Model

Trusted Position is formalized as a freshness-constrained property: a position message is consistent only if it arrives within a budget compatible with the on-board refresh context. For a 10-15 Hz pipeline, $T_{\mathrm{DOD}} \approx 0.067$–$0.10$ s. The freshness condition is:

$$D_{\mathrm{net}} \;\leq\; \alpha\, T_{\mathrm{DOD}}, \tag{3}$$

where $\alpha \geq 1$ captures how many perception cycles may elapse before the communicated position becomes stale. α=1 enforces strict single-cycle coherence (67-100 ms); α=3 allows a 200–300 ms budget where a few missed cycles are tolerable. The staleness probability and freshness margin are:

$$P_{\mathrm{stale}} \;=\; P(D_{\mathrm{net}} > \alpha\, T_{\mathrm{DOD}})\,, \tag{4}$$

$$M_{\mathrm{fresh}} \;=\; \alpha\, T_{\mathrm{DOD}} - \mu_D, \tag{5}$$

where non-positive margins indicate a non-negligible fraction of stale messages. The same delay statistics govern the QPV verification-bound layer: schedulers that violate the freshness budget simultaneously render external position verification infeasible at urban-scale verifier geometries.

QPV Verification-Bound Layer

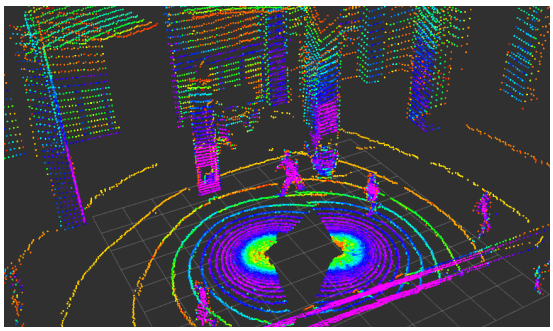
QPV is incorporated as an abstract, timing-bound constraint rather than an implemented subsystem. A prover convinces distributed verifiers of its location by meeting strict relativistic timing constraints Miller & Alnawakhtha (2024); Kent et al. (2011); even with high-quality on-board perception, external verification can be fundamentally limited by communication timing alone. QPV succeeds only if the communication delay remains within an admissible window W_{QPV}, a few to tens of milliseconds for urban verifier separations of hundreds of meters to a few kilometers:

$$D_{\mathrm{net}} \leq W_{\mathrm{QPV}} \;\Rightarrow\; \text{feasible}, \qquad D_{\mathrm{net}} > W_{\mathrm{QPV}} \;\Rightarrow\; \text{infeasible}, \tag{6}$$

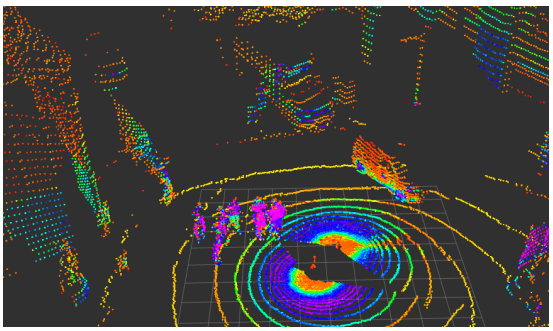
with failure probability:

$$P_{\mathrm{fail}}^{\mathrm{QPV}} = P(D_{\mathrm{net}} > W_{\mathrm{QPV}})\,. \tag{7}$$

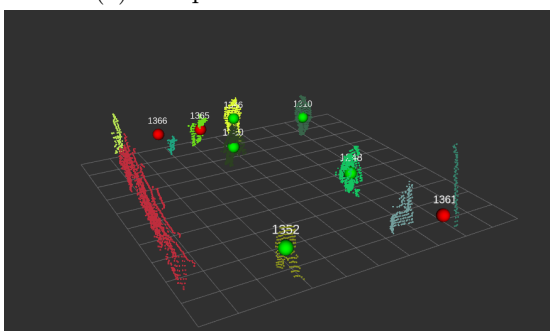
Higher jitter and tail delay increase $P_{\mathrm{fail}}^{\mathrm{QPV}}$ even at moderate mean delay Escolà-Farràs & Speelman (2023), reinforcing QPV as a constraint-driven layer rather than a plug-in guarantee.



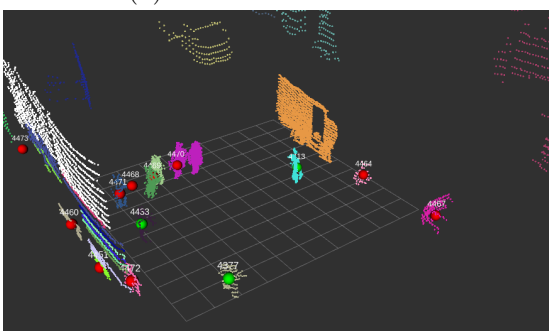
(a) Campus Nord: raw LiDAR.



(b) El Born: raw LiDAR.



(c) Campus Nord: DOD output.



(d) El Born: DOD output.

Figure 4: Qualitative DOD evidence on ONA: raw LiDAR inputs and corresponding pipeline outputs in Campus Nord and El Born deployments.

Table 3: Validated on-board DOD performance summary on ONA (real-world deployments).

Metric	**Observed value**
Operating rate	10-15 Hz
Static filtering accuracy	>80%
Dynamic tracking (with static filtering)	∼45-50%
Dynamic tracking (without static filtering)	∼20%

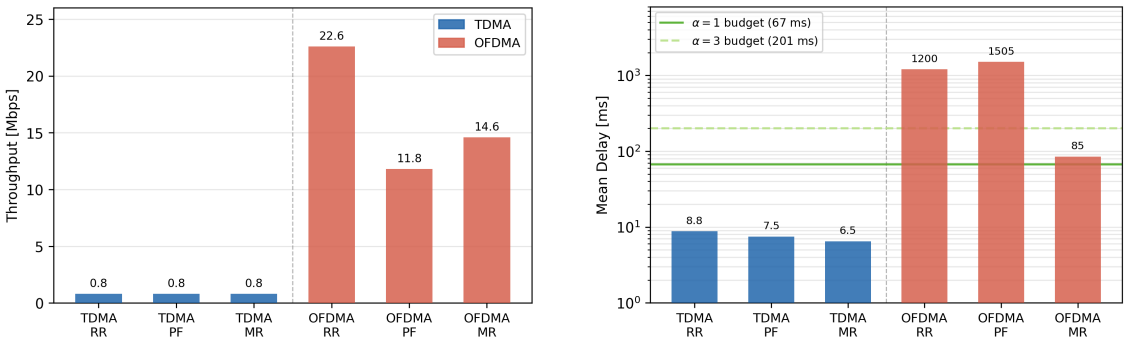
3 Results and Discussion

DOD Pipeline Performance

The DOD pipeline was evaluated across two contrasting urban settings: Campus Nord (semi-structured academic environment) and El Born (dense historical city center of Barcelona). Figure 4 shows raw LiDAR inputs and DOD outputs. The pipeline maintained 10-15 Hz operation, achieved >80% static filtering accuracy, and approximately 45-50% dynamic tracking accuracy with ego-motion compensation enabled Küçükali et al. (2025); without Stage 4, accuracy drops to 20%. These results establish a reliable on-board timing reference independent of connectivity. Table 3 summarizes validated performance metrics.

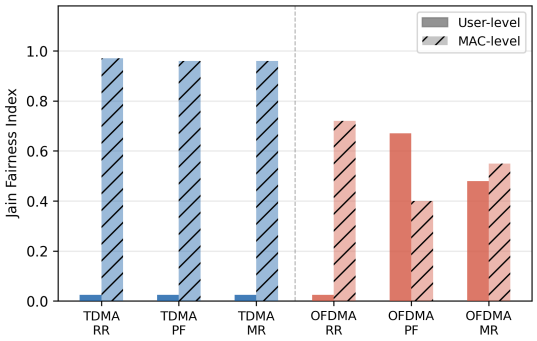
5G Scheduler Performance Under Urban Mobility

Figure 5 presents the global scheduler comparison under SUMO-based urban vehicular mobility. A clear performance gap separates TDMA and OFDMA across all three KPIs, intensified by the 150 UE load driving OFDMA schedulers into severe resource contention. TDMA delivers consistent throughput of ≈0.8 Mbps with stable mean delays of 6-9 ms, since frequency-domain multiplexing is absent. OFDMA schedulers reach substantially higher throughput but at a severe latency cost: OFDMA PF drives mean delay



(a) Total throughput.

(b) Mean user delay.



(c) Jain fairness index.

Figure 5: Global scheduler comparison under SUMO-based urban vehicular mobility: throughput, mean delay, and dual-level Jain fairness across all six TDMA/OFDMA × {RR, PF, MR} configurations. Delay is shown on a logarithmic scale; green lines mark the α=1 (67 ms) and α=3 (201 ms) freshness budgets. Solid bars show user-level fairness; hatched bars show MAC-level fairness.

to ≈1505 ms, OFDMA RR produces comparably elevated delays due to queue growth, and OFDMA MR is the sole exception at ≈85 ms through channel-quality-driven allocation.
Jain fairness reveals a dual-level distinction. MAC fairness measures resource allocation equality; user-level fairness reflects delivered throughput. TDMA yields near-perfect MAC fairness (0.96-0.97) but low user throughput fairness (≈0.024); OFDMA PF improves user-level fairness (≈0.67) through adaptive allocation.
Table 4 shows that scheduler choice shifts the system across freshness boundaries. All TDMA policies produce nearly identical throughput and delay, confirming negligible policy impact without frequency-domain multiplexing. Among OFDMA configurations, RR maximizes throughput but incurs highest delay and lowest user fairness; PF trades throughput for fairness at 1505 ms; MR is the sole OFDMA candidate for position-freshness compatibility. TDMA's near-perfect MAC fairness (0.96-0.97) versus low user-throughput fairness (≈0.024) has direct implications for multi-robot deployments.

Freshness and QPV Feasibility Analysis

With $T_{\mathrm{DOD}} \approx 0.067$–$0.10$ s, TDMA schedulers (6–9 ms) remain well within the strict single-cycle freshness budget (α=1: 67–100 ms) under all policies, yielding a positive margin of around 60 ms. OFDMA MR at ≈85 ms violates strict coherence but satisfies the relaxed tolerance (α=3, budget 201–300 ms), adopted here as a multi-cycle robustness margin, and is therefore the only OFDMA configuration compatible with trusted positioning under the relaxed freshness criterion. OFDMA PF at 1505 ms and OFDMA RR at ≈1200 ms remain infeasible under any tolerance setting, exceeding the most relaxed budget by over 1.0 s and 1.3 s respectively. Table 5 and Figure 6 summarize the feasibility analysis.

Table 4: Per-scheduler KPI summary under SUMO-based urban vehicular mobility conditions.

Scheduler	**Throughput [Mbps]**	**Mean Delay [ms]**	**User Jain**	**MAC Jain**
TDMA RR	≈0.8	≈8.8	0.024	0.97
TDMA PF	≈0.8	≈7.5	0.024	0.96
TDMA MR	≈0.8	≈6.5	0.024	0.96
OFDMA RR	≈22.6	≈1200	0.024	0.72
OFDMA PF	≈11.8	≈1505	0.67	0.40
OFDMA MR	≈14.6	≈85	0.48	0.55

Table 5: Freshness feasibility analysis.

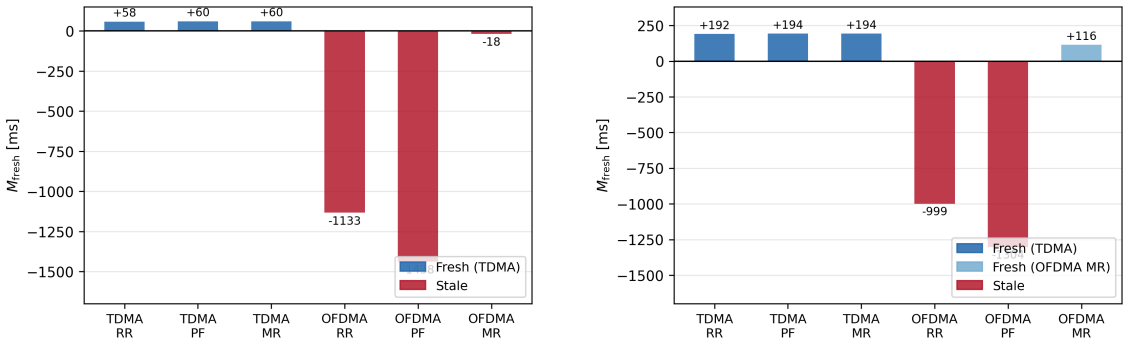
Case	T_{DOD}	α	**Feasible schedulers**
Strict coherence	0.067–0.10 s	1	TDMA all; OFDMA: none
Multi-cycle (fast)	0.067 s	3	TDMA all; OFDMA MR only
Multi-cycle (slow)	0.10 s	3	TDMA all; OFDMA MR only

For urban-scale verifier separations of hundreds of meters to a few kilometers, W_{QPV} lies in the range of a few to tens of milliseconds. TDMA schedulers (6–9 ms) remain within feasible QPV windows across all policies, making them the only configurations compatible with both freshness and external position verification within the proposed timing-bound model. OFDMA MR (≈85 ms) satisfies the relaxed freshness budget but falls outside the QPV admissible window, yielding a three-tier trust classification: TDMA schedulers are trusted (fresh and QPV-feasible); OFDMA MR is conditionally trusted (fresh under α=3, QPV-infeasible); and OFDMA PF/RR are untrusted under all criteria. In this sense, the observed delay statistics provide an operational interpretation of $P_{\mathrm{fail}}^{\mathrm{QPV}}$ from Eq. (7) without requiring QPV hardware.

Four design guidelines follow. First, TDMA should be preferred for delay-sensitive position interactions, maintaining sub-10 ms delivery across all policies. Second, if OFDMA is required for capacity, MR is the only viable policy under the relaxed freshness criterion, providing a 17× delay reduction relative to PF, although QPV-incompatible. Third, RR should be avoided under OFDMA in loaded urban networks, as it combines severely elevated delay with the lowest user-level fairness. Fourth, scheduling must be evaluated at the application service level, since MAC-level fairness does not translate into throughput fairness under heterogeneous channel conditions. Trusted positioning with QPV-based verification is achievable under TDMA when configuration choices align with the robot's perception refresh rhythm.

4 Conclusions

This work introduced a three-layer Trusted Position framework: a validated LiDAR-IMU DOD pipeline, a 5G connectedness envelope characterized under SUMO-based urban vehicular mobility, and an abstract QPV-inspired timing-bound constraint. The DOD subsystem on ONA achieves 10-15 Hz operation with >80% static filtering and up to 50% dynamic tracking accuracy. ns-3/5G-LENA simulations revealed a clear throughput–timeliness trade-off: OFDMA schedulers drive mean delays to 85–1505 ms depending on policy, while TDMA maintains sub-10 ms delivery and remains trusted under both fresh-



(a) Strict coherence: α=1, budget = 67 ms.

(b) Multi-cycle coherence: α=3, budget = 201 ms.

Figure 6: Freshness margin $M_{\text{fresh}} = \alpha T_{\text{DOD}} - \mu_D$ per scheduler and access-mode configuration. Bars above zero are fresh; bars below are stale. Blue: TDMA (fresh under all cases). Light blue: OFDMA MR (conditionally fresh under α=3 only). Red: stale.

ness and QPV constraints; OFDMA MR is conditionally trusted, and PF/RR are infeasible under all criteria. A secondary finding is that MAC-level and user-level throughput fairness diverge significantly under heterogeneous channel conditions, with direct implications for multi-robot deployments. Trusted positioning is fundamentally governed by temporal coherence between perception refresh and network delivery, preservable through deliberate scheduler and access-mode selection without continuous perception streaming.
Future work should validate the framework on a real 5G testbed with ONA in the loop, and extend the DOD pipeline with camera-based semantic inputs to close the dynamic tracking accuracy gap. On the network side, Age-of-Information-aware scheduling and QPV analysis extended to delay tail distributions would move beyond mean-delay estimates toward probabilistic position trust guarantees.

Acknowledgements

This work was carried out within CARNET (UPC, SEAT, and Volkswagen Group Innovation) and the Universitat Politècnica de Catalunya. This research was supported by the Spanish Government under grants MCIU PDR-2014-2022/56-30157-2021-2A, Metropolis PLEC2021-007609, PID2022-136869NB-C31, PID2022-136869NB-C32, PDC2022-333091-I00, RED2024-154236, PID2022-137329OB-C41, and CNS2024-154600. The latter two were funded under MICIU/AEI/10.13039/501100011033/FEDER (UE) of the Agencia Estatal de Investigación (Spain). Additional support was provided by the Catalan Government University and Research Aid Management Agency (AGAUR) under Research Group grants 2021 SGR 01415 Q0818003F and 2021 SGR 01046. Additional funding was provided by the European Union project 101203230 (CERTAIN), project 101147397 (CulturalRoad), and the project Ajuda RED2024-154236-E, funded by MICIU/AEI (10.13039/501100011033). Furthermore, the research has also been developed in the context of the following project: AgríLogistics, funded by TSI-100123-2024-70 and by the European Union NextGenerationEU/PRTR. The authors wish to formally acknowledge these projects for their role in supporting the broader research context in which this study has been conducted. The authors also thank the ONA platform team for access to the robot and urban deployment context, as well as colleagues who contributed to the simulation and analysis discussions.

References

3GPP. (2021). *NR; radio resource control (RRC) protocol specification* (Tech. Rep. No. TS 38.331). 3rd Generation Partnership Project. Retrieved from `https://www.3gpp.org/ftp/Specs/archive/38_series/38.331/`

5G-LENA Project. (2019). *5G-LENA: 5G NR module for the ns-3 simulator.* Retrieved from

https://5g-lena.cttc.es/ (Accessed 2026-02-25)

Cibir, E., Birgul, U., & Atali, G. (2024, 12). High-frequency ground segmentation for autonomous mobile robots: A ransac-based approach. *The European Journal of Research and Development*, *4*, 309-315. Retrieved from https://doi.org/10.56038/ejrnd.v4i4.527 doi: 10.56038/ejrnd.v4i4.527

Du, W., & Beltrame, G. (2024, 07). Lidar-based real-time object detection and tracking in dynamic environments. Retrieved from https://arxiv.org/abs/2407.04115 doi: 10.48550/arXiv.2407.04115

Escolà-Farràs, L., & Speelman, F. (2023, October). Single-qubit loss-tolerant quantum position verification protocol secure against entangled attackers. *Phys. Rev. Lett.*, *131*, 140802. Retrieved from https://link.aps.org/doi/10.1103/PhysRevLett.131.140802 doi: 10.1103/PhysRevLett.131.140802

Jain, R., Chiu, D.-M., & Hawe, W. R. (1984). A quantitative measure of fairness and discrimination. *DEC Research Report*. Retrieved from https://www.cse.wustl.edu/~jain/papers/ftp/fairness.pdf

Jiang, W., Song, C., Wang, H., Yu, M., & Yan, Y. (2023, 01). Obstacle detection by autonomous vehicles: An adaptive neighborhood search radius clustering approach. *Machines*, *11*, 54. Retrieved from https://doi.org/10.3390/machines11010054 doi: 10.3390/machines11010054

Kaul, S., Yates, R., & Gruteser, M. (2012, March). Real-time status: How often should one update? In *Proceedings of ieee infocom* (pp. 2731–2735). Orlando, FL. Retrieved from https://doi.org/10.1109/INFCOM.2012.6195689 doi: 10.1109/INFCOM.2012.6195689

Kent, A., Munro, W. J., & Spiller, T. P. (2011, July). Quantum tagging: Authenticating location via quantum information and relativistic signaling constraints. *Phys. Rev. A*, *84*, 012326. Retrieved from https://link.aps.org/doi/10.1103/PhysRevA.84.012326 doi: 10.1103/PhysRevA.84.012326

Küçükali, E., Pages, L., Ferrando-Bataller, M., & Jofre-Roca, L. (2025, August). Lidar–imu perception for real-time dynamic obstacle detection in complex urban environments. In *Proceedings of the international conference on urban freight transportation and distribution (icuftd-25)*. Melbourne, Australia. Retrieved from https://academicresearchlibrary.com/storage/pdf/KZvYagpa5H4X3N4g09mSM8JQonP6jkgZloHO5F2A.pdf (Accessed 2026-02-26)

Leong, P., & Ahmad, N. (2024, 01). Lidar-based obstacle avoidance with autonomous vehicles: A comprehensive review. *IEEE Access*, *PP*, 1-1. Retrieved from https://doi.org/10.1109/ACCESS.2024.3493238 doi: 10.1109/ACCESS.2024.3493238

Li, J., Zhang, Y., Liu, X., Zhang, X., & Bai, R. (2021, 08). Obstacle detection and tracking algorithm based on multi-lidar fusion in urban environment. *IET Intelligent Transport Systems*, *15*. Retrieved from https://doi.org/10.1049/itr2.12105 doi: 10.1049/itr2.12105

Lin, Z., Chuanli, K., Wu, S., Li, X., Cai, L., Zhang, D., & Wang, S. (2024, 01). Adaptive clustering for point cloud. *Sensors*, *24*, 848. Retrieved from https://doi.org/10.3390/s24030848 doi: 10.3390/s24030848

Lopez, P. A., et al. (2018). *SUMO – simulation of urban MObility.* Retrieved from https://sumo.dlr.de (Version 1.0)

Miller, C., & Alnawakhtha, Y. (2024, 06). Perfect cheating is impossible for single-qubit position verification. Retrieved from https://arxiv.org/abs/2406.20022 doi: 10.48550/arXiv.2406.20022

Mills-Tettey, G. A., Stentz, A., & Dias, M. B. (2007, July). *The dynamic hungarian algorithm for the assignment problem with changing costs* (Tech. Rep. No. CMU-RI-TR-07-27). Pittsburgh, PA: Robotics Institute, Carnegie Mellon University. Retrieved from https://www.ri.cmu.edu/pub_files/pub4/mills_tettey_g_ayorkor_2007_3/mills_tettey_g_ayorkor_2007_3.pdf

Rosique, F., Navarro Lorente, P., Fernandez, C., & Padilla, A. (2019, 02). A systematic review of perception system and simulators for autonomous vehicles research. *Sensors*, *19*, 648. Retrieved from https://doi.org/10.3390/s19030648 doi: 10.3390/s19030648

Sualeh, M., & Kim, G.-W. (2020, 08). Visual-lidar based 3d object detection and tracking for embedded systems. *IEEE Access*. Retrieved from https://doi.org/10.1109/ACCESS.2020.3019187 doi: 10.1109/ACCESS.2020.3019187

Trabelsi, N., Chaari Fourati, L., & Chen, C. S. (2024). Interference management in 5G and beyond networks. *arXiv preprint arXiv:2401.01608*. Retrieved from https://arxiv.org/abs/2401.01608

Xie, D., Xu, Y., & Wang, R. (2019, 03). Obstacle detection and tracking method for autonomous vehicle based on three-dimensional lidar. *International Journal of Advanced Robotic Systems*, *16*, 172988141983158. Retrieved from https://doi.org/10.1177/1729881419831587 doi: 10.1177/1729881419831587